

Research Article

Multicentennial to millennial-scale changes in the East Asian summer monsoon during Greenland interstadial 25

Jinguo Dong^{a*}, Chuan-Chou Shen^{b,c*}, Yi Wang^d, Hsun-Ming Hu^{b,c}, Yogaraj Banerjee^{b,c} and Wei Huang^e

^aCollege of Geosciences, Nantong University, Nantong 226007, PRC; ^bHigh-Precision Mass Spectrometry and Environment Change Laboratory (HISPEC), Department of Geosciences, National Taiwan University, Taipei 10617, Taiwan, ROC; ^cResearch Center for Future Earth, National Taiwan University, Taipei 10617, Taiwan, ROC; ^dDepartment of Geography, School of Global Studies, University of Sussex, Brighton BN1 9QJ, UK and ^eDepartment of Geographical Science, Yichun University, Yichun 336000, PRC

Abstract

A multidecadal-resolved stalagmite $\delta^{18}\text{O}$ record from two nearby caves, Lianhua and Dragon, in Shanxi Province, northern China, characterizes the detailed East Asian summer monsoon (EASM) intensity changes at 114.6–108.3 ka during Marine Oxygen Isotope Stage 5d. Our record shows an intensification of the EASM at 114.6–109.5 ka, followed by a rapid weakening at 109.5–108.4 ka. The millennial-scale strong monsoonal event appears to be correlated with the warm Greenland interstadial 25 (GI 25), whereas the weak monsoonal event is related to the cold Greenland stadial 25 within dating errors. The GI 25 monsoonal event registered in our record is also documented in various published time series from different regions of China. The lines of evidence indicate that this event occurred over the entirety of monsoonal China and was also broadly antiphase, similar to the corresponding event on a millennial time scale in the South American monsoon territory. In our record, one 700 yr weak monsoon event at $110.7^{+0.6}_{-0.5}$ to $110.0^{+0.8}_{-0.4}$ ka divides the GI 25 into three substages. These multicentennial to millennial-scale monsoon events correspond to two warm periods and an intervening cold interval for the intra-interstadial climate oscillations within GI 25, thus supporting a persistent coupling of the high- and low-latitude climate systems over the last glacial period.

Keywords: East Asian summer monsoon, North Atlantic, Stalagmite, Millennial–centennial scale event, Marine Oxygen Isotope Stage 5d, Greenland interstadial 25, Greenland stadial 25

(Received 1 June 2021; accepted 14 January 2022)

INTRODUCTION

The transition from the last interglacial to the last glacial period occurred between ~120 and 110 thousand years ago (ka, before AD 1950) and was characterized by progressive ice-sheet growth in response to the climatic amplification of astronomical forcing through the Earth's internal feedback (Landais et al., 2006; Capron et al., 2010, 2012 and references therein). At least one-quarter of ice-sheet volume during full glacial conditions was reached during Marine Oxygen Isotope Stage (MIS) 5d. This transition is also associated with an abrupt millennial-scale warming event first identified in North Atlantic marine records (Chapman and Shackleton, 1999; Oppo et al., 2006), identified as Dansgaard-Oeschger (DO) event 25 in the NGRIP $\delta^{18}\text{O}$ record (NGRIP Project Members, 2004).

DO events are one of the classical features of the last glacial period (NGRIP Project Members, 2004). A DO event in

Greenland is described as an abrupt warming of 8°C–16°C within a few decades (Kindler et al., 2014 and references therein), leading to peak interstadial conditions, Greenland interstadial (GI), followed by a gradual cooling, and finally ending in rapid return to the cold stadial state, Greenland Stadial (GS). These abrupt climate changes have been recorded in numerous paleoclimatic archives worldwide (Porter and An, 1995; Chapman and Shackleton, 1999; Leuschner and Sirocko, 2000; Wang et al., 2001; Voelker, 2002; NGRIP Project Members, 2004; EPICA Community Members, 2006; Zhao et al., 2010; Baumgartner et al., 2014; Zhang et al., 2020) and persisted through the entire last glacial period.

As an abrupt climate event during the MIS 5d, GI 25 is very similar in pattern and transition to those observed during MIS 3 in the Greenland ice-core $\delta^{18}\text{O}$ record (NGRIP Project Members, 2004; Rasmussen et al., 2014). Climate excursions are also clearly registered in cave records from southern Europe, providing the first direct, independent, and radiometrically derived estimates for the timing of GI 25 and GI 24 (Drysdale et al., 2007; Boch et al., 2011; Columbu et al., 2017; Moseley et al., 2020). A detailed comparison of the NGRIP record with multiple indicators shows GI 25 does not match hydroclimate changes at low-latitude zones (Capron et al., 2012). Such an equivocal fingerprint raises the question of whether GI 25 is simply a rapid event.

*Corresponding authors at: College of Geosciences, Nantong University, Nantong, China. E-mail address: dongjinguo1111@163.com (J. Dong). HISPEC, Department of Geosciences, National Taiwan University, Taipei, Taiwan, ROC. E-mail address: river@ntu.edu.tw (C.-C. Shen).

Cite this article: Dong J, Shen C-C, Wang Y, Hu H-M, Banerjee Y, Huang W (2022). Multicentennial to millennial-scale changes in the East Asian summer monsoon during Greenland interstadial 25. *Quaternary Research* 109, 195–206. <https://doi.org/10.1017/qua.2022.5>

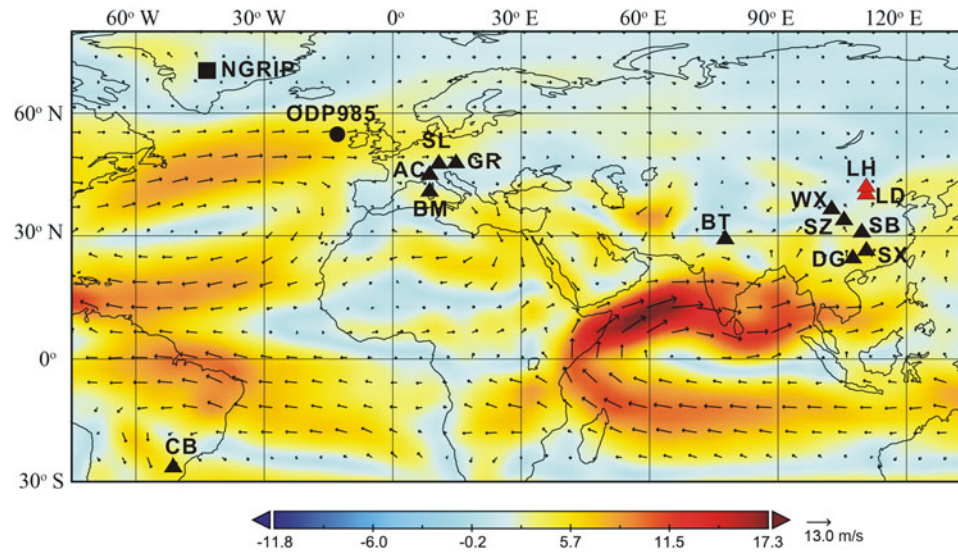


Figure 1. A world map with summer (June–July–August) mean 850 hPa vector wind based on the National Centers for Environmental Prediction/National Center for Atmospheric Research (NCEP/NCAR) Reanalysis (1960–2020). The red triangles represent the Lianhau (LH), and Dragon Caves (LD) (this study). Black triangles represent the Sanbao (SB; Wang et al., 2008), Wanxiang (WX; Johnson et al., 2006), Suozi (SZ; Zhou et al., 2008), Dongge (DG; Yuan et al., 2004; Kelly et al., 2006), Sanxing (SX; Jiang et al., 2016), and Bittoo (BT; Kathayat et al., 2016) Caves in the southeastern Asian monsoon region; Schneckthe loch (SL; Moseley et al., 2020), Grete-Ruth shaft (GR; Boch et al., 2011), Antrodrl-Corchia (AC; Drysdale et al., 2007), and Bue Marino (BM; Columbu et al., 2017) Caves in southern Europe nearby the Mediterranean Sea; and Caverna Botuverá Cave (CB; Cruz et al., 2005) in Brazil, South America. The black dot represents the International Ocean Discovery Program sediment core (ODP) 985 (Oppo et al., 2006); and the black square represents the North Greenland Ice Core Project (NGRIP; NGRIP Members, 2004). The Asian summer monsoon is a steady flow of warm, moist air from the tropical oceans, while the winter monsoon is a flow of cold, dry air associated with the Siberian–Mongolian High.

Interestingly, two high-resolution stalagmite $\delta^{18}\text{O}$ records from Sanbao Cave in central China and Bittoo Cave in northern India provided unambiguous evidence of a strengthened GI 25 monsoon event at MIS 5d, concurring with the contemporaneous event in the Greenland $\delta^{18}\text{O}$ record (Wang et al., 2008; Kathayat et al., 2016). But records from the caves of Suozi (Zhou et al., 2008) and Wanxiang (Johnson et al., 2006) in monsoonal China show no clear evidence for this abrupt event (Fig. 1). Thus, there is still a debate whether the decoupling between low- and high-latitude climate conditions occurred during the last glacial inception (Zhou et al., 2008; Wu et al., 2020).

Recently, significant and rapid cold–warm climate oscillations within DO events have been documented in Greenland ice cores, especially during MIS 5 (Capron et al., 2010; Rasmussen et al., 2014). Such multicentennial-scale climate excursions were also reported in Alpine cave records (Boch et al., 2011), southern Italian lacustrine sediments (Martin-Puertas et al., 2014), and Mediterranean cave deposits (Columbu et al., 2017). For example, a high-resolution cave record from Sardinia first revealed a cool-dry to warm-wet oscillation independently associated with the first intra-GI/GS events GI 25a–c (Columbu et al., 2017). However, no proxy record with detailed structure for DO 25 in the low-latitude Asian monsoon region is available. To fully understand the monsoonal climate variability on multicentennial-to-millennial scales, high-resolution and precisely dated cave records are required.

Here, we report a multidecadally resolved stalagmite $\delta^{18}\text{O}$ record from the Lianhua and Dragon Caves in northern China, near the eastern boundary of the Chinese Loess Plateau (CLP), where very limited well-dated proxy records are currently available. High resolution sampling and more U–Th dates with uncertainties of ± 100 s yr allows us to reconstruct the East Asian summer monsoon (EASM) evolution at multicentennial-to-millennial time scales during MIS 5d. Our new Lianhua–Dragon records

show millennial-scale GI/GS 25 monsoon events occurring at 114.6–108.3 ka, substages of intra-interstadial oscillations of the GI 25 monsoon event, and the linkage to low- and high-latitude hydroclimates at MIS 5d.

STUDY SITE

Two caves, Lianhua ($38^{\circ}10'N$, $113^{\circ}43'E$, 1200 m above sea level [m asl]) and Dragon ($36^{\circ}46'N$, $113^{\circ}13'E$, 1600 m asl), 150 km apart in Shanxi Province, northern China, were selected for the present study (Fig. 1). Both caves had small entrances, 1 m in height and 2 m in width, and developed in the same carbonate bedrock, Ordovician limestone. Their narrow passages, 1–2 m in height, were 250 and 1000 m long, respectively. Relative humidity in the inner part, 170 m to the cave entrance, reaches 98%–100% in both caves. The overlying soil layer on the limestone above the caves is thin, only 0–1 m, favorable to rapidly communicate the external climate signal into the cave (Dong et al., 2015, 2018a). The EASM strongly influences this area, and the hydroclimate is characterized by warm-wet summers and cool-dry winters. The region receives maximum precipitation (almost 75% of the annual rainfall) between June and September when the summer monsoon prevails (Dong et al., 2015, 2018a, 2018b).

Local ground air temperature for Lianhua Cave is 11.0°C , and annual precipitation is 515 mm (AD 1970–AD 2000; recorded in a meteorological station Yangquan, 20 km from the cave). For Dragon Cave, the local air temperature is 10.3°C , and the local annual precipitation is 530 mm (AD 1970–AD 2000; meteorological station Wuxiang, 18 km from the cave).

SAMPLES AND METHODS

One stalagmite, LH36, 206 mm in length and 80–110 mm in diameter, was collected in a chamber 200 m from the entrance of

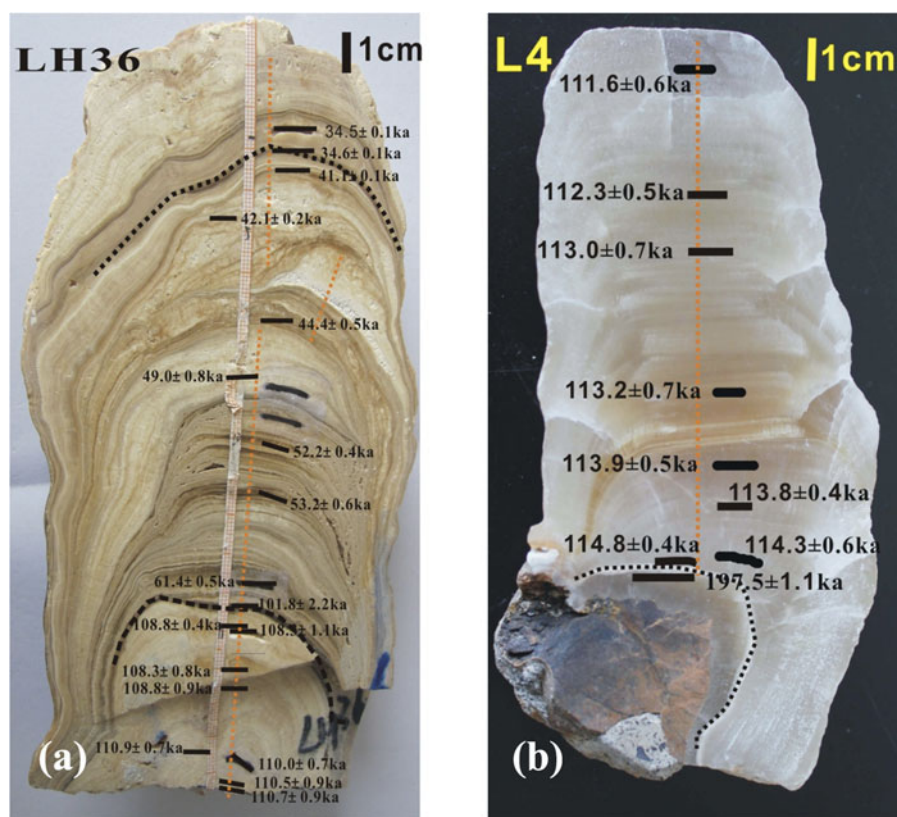


Figure 2. Photographs of stalagmite samples (a) LH36 of Lianhua Cave and (b) L4 of Dragon Cave. Horizontal layers denote the subsamples drilled for U-Th dating. Black dashed lines represent the depositional hiatuses. Orange vertical dashed lines show the paths for carbon and oxygen isotopic measurement.

Lianhua Cave. Another stalagmite, L4, 126 mm in length and 55–70 mm in diameter, was collected in the gallery 600 m from the entrance of Dragon Cave. Both stalagmites were sectioned along the vertical growth axis using a water-cooled saw (Fig. 2). For LH36, alternating changes of the petrography are observed at 33–35 and 153–155 mm intervals from the top (Fig. 2a), indicating possible growth discontinuities. The lower part from 155–206 mm is characterized with milky-white layering. Stalagmite L4 is very clean and composed of transparent and compact calcite throughout the whole growing period. Only one white clay lamina is observed at 115 mm from the top, suggesting a possible hiatus (Fig. 2b).

Twenty-eight subsamples, 19 from LH36 and 9 from L4 (Fig. 2, Table 1), with a weight range from 100 to 200 mg, were drilled parallel to the growth plane for U-Th chemistry (Shen et al., 2003) and dating (Shen et al., 2002, 2012). U-Th isotopic measurement was performed on a multicollector inductively coupled plasma mass spectrometer (MC-ICP-MS), Thermo Finnigan NEPTUNE, housed at the High-Precision Mass Spectrometry and Environment Change Laboratory (HISPEC), Department of Geosciences, National Taiwan University, and at the Nanjing Normal University Isotope Laboratory (Shen et al., 2012; Shao et al., 2019). A gravimetrically calibrated (Cheng et al., 2013) triple-spike, ^{229}Th - ^{233}U - ^{236}U , isotope-dilution method was applied to correct the mass bias and determine the U-Th contents and isotopic compositions (Shen et al., 2012). Uncertainties in isotopic data and dates relative to AD 1950, are given at the 2σ level or 2 standard deviations of the mean ($2\sigma_m$). Half-lives of nuclides used for age calculation are given in Cheng et al. (2013). StalAge algorithm techniques (Scholz and Hoffmann, 2012) were used to construct the age models.

For stable isotope analysis, carbonate subsamples were drilled out with a 0.3-mm-diameter carbide dental bur at 1 mm intervals for the upper segment (30–153 mm) and at 0.5 mm intervals for the lower part (153–206 mm) of stalagmite LH36. Subsamples were retrieved at 1 mm intervals for the depth range of 0–116 mm for stalagmite L4 (Fig. 2). Stable isotope analysis was carried out on 340 powdered samples (Supplementary Table 1), each weighing 20–40 μg , using a Finnigan-MAT 253 mass spectrometer equipped with an automated Kiel Carbonate Device at the College of Geography Science, Nanjing Normal University. Carbonate $\delta^{18}\text{O}$ (‰) values are expressed relative to the Vienna Pee Dee Belemnite (VPDB) reference standard. An international standard, NBS-19, was measured every 15–20 subsamples to confirm that a 6 month 1-sigma external error was better than $\pm 0.06\%$ for $\delta^{18}\text{O}$.

RESULTS

Chronology

The U-Th isotopic composition, content, and ^{230}Th dates were determined are listed in Table 1. Relatively low ^{238}U content of 0.09 – 0.34×10^{-6} g/g and high ^{232}Th of 10^{-1} – $10^2 \times 10^{-9}$ g/g in LH36 layers result in age uncertainties of ± 0.1 – 2.2 ka. Most (16/19) of the corrected ^{230}Th ages are in stratigraphic order. StalAge algorithm techniques (Scholz and Hoffmann, 2012) show an age model from 34.6 ± 0.1 to 110.7 ± 0.9 ka, with two growth hiatuses at depths of 33–35 and 153–155 mm from the top (Fig. 2), identified at 34.6 – 41.1 and 61.4 – 108.0 ka, respectively (Fig. 3). The calculated deposition rates are $6 \mu\text{m}/\text{yr}$ for the upper section at 40–150 mm and $21 \mu\text{m}/\text{yr}$ for the lower section at 155–206 mm for stalagmite LH36.

Table 1. Uranium and thorium isotopic compositions and ^{230}Th ages for stalagmites L4 (Dragon Cave) and LH36 (Lianhua) using a multicollector inductively coupled plasma mass spectrometer MC-ICP-MS.

ID/ depth (mm) ^a	^{238}U 10^{-6}g/g^b	^{232}Th 10^{-9}g/g	$\delta^{234}\text{U}$ measured ^b	$^{230}\text{Th}/^{238}\text{U}$ activity ^c	$^{230}\text{Th}/^{232}\text{Th}$ atomic ($\times 10^{-3}$)	$\delta^{234}\text{U}$ initial ^d	Age (ka BP) uncorrected	Age (ka BP) corrected ^{c,e,f}
LH36-27	0.1335 ± 0.0002	1.3 ± 0.006	2113 ± 4	0.875 ± 0.003	1.479 ± 0.008	2329 ± 5	34.6 ± 0.1	34.6 ± 0.1
LH36-33	0.2334 ± 0.0003	0.281 ± 0.006	1922 ± 3	0.822 ± 0.002	11.26 ± 0.24	2120 ± 3	34.7 ± 0.1	34.6 ± 0.1
LH36-37*	0.1619 ± 0.0001	2.6 ± 0.02	1571 ± 2	0.839 ± 0.002	0.861 ± 0.008	1765 ± 3	41.2 ± 0.1	41.1 ± 0.1
LH36-51	0.9751 ± 0.0001	2.1 ± 0.01	1474 ± 3	0.825 ± 0.003	0.635 ± 0.003	1660 ± 3	42.4 ± 0.2	42.1 ± 0.2
LH36-80*	0.1346 ± 0.0001	21.3 ± 0.11	1630 ± 1	0.956 ± 0.002	0.100 ± 0.001	1851 ± 5	46.8 ± 0.1	45.2 ± 0.8
LH36-80	0.0956 ± 0.0001	8.0 ± 0.03	1630 ± 3	0.929 ± 0.006	0.183 ± 0.001	1849 ± 5	45.3 ± 0.4	44.4 ± 0.5
LH36-95	0.1026 ± 0.0001	11.5 ± 0.05	1196 ± 4	0.842 ± 0.006	0.124 ± 0.001	1373 ± 5	50.3 ± 0.5	49.0 ± 0.8
LH36-113	0.1569 ± 0.0002	8.1 ± 0.03	2478 ± 4	1.400 ± 0.007	0.448 ± 0.003	2873 ± 6	52.7 ± 0.3	52.2 ± 0.4
LH36-127	0.1409 ± 0.0002	11.6 ± 0.06	1500 ± 3	1.021 ± 0.007	0.205 ± 0.002	1743 ± 5	54.1 ± 0.5	53.2 ± 0.6
LH36-147	0.2570 ± 0.0004	10.7 ± 0.04	991 ± 3	0.899 ± 0.005	0.356 ± 0.002	1179 ± 4	61.9 ± 0.4	61.4 ± 0.5
LH36-154	0.1546 ± 0.0002	66.4 ± 0.3	2139 ± 5	2.12 ± 0.02	0.081 ± 0.001	2851 ± 19	104.8 ± 1.7	101.8 ± 2.2
LH36-157	0.3371 ± 0.0004	0.764 ± 0.006	850 ± 3	1.244 ± 0.002	9.05 ± 0.07	1156 ± 4	108.9 ± 0.4	108.8 ± 0.4
LH36-158	0.314 ± 0.001	2.53 ± 0.01	852 ± 7	1.243 ± 0.006	2.55 ± 0.01	1157 ± 11	108 ± 1	108 ± 1
LH36-170	0.2993 ± 0.0004	7.39 ± 0.01	903 ± 3	1.281 ± 0.005	0.856 ± 0.004	1226 ± 5	108.7 ± 0.8	108.3 ± 0.8
LH36-175	0.2663 ± 0.0004	5.16 ± 0.01	823 ± 4	1.227 ± 0.006	1.045 ± 0.005	1119 ± 6	109.2 ± 0.9	108.9 ± 0.9
LH36-195	0.2849 ± 0.0004	8.17 ± 0.02	874 ± 2	1.280 ± 0.007	0.736 ± 0.004	1195 ± 4	111.4 ± 0.9	111.0 ± 0.9
LH36-197	0.2790 ± 0.0004	3.401 ± 0.009	853 ± 4	1.256 ± 0.004	1.700 ± 0.006	1164 ± 7	110.2 ± 0.7	110.0 ± 0.7
LH36-202	0.2711 ± 0.0007	5.37 ± 0.01	844 ± 6	1.251 ± 0.005	1.042 ± 0.004	1152 ± 8	110.5 ± 0.9	110.2 ± 0.9
LH36-204	0.2543 ± 0.0006	4.68 ± 0.01	844 ± 5	1.255 ± 0.005	1.126 ± 0.005	1153 ± 7	111.0 ± 0.9	110.7 ± 0.9
L4-10	1.618 ± 0.003	0.056 ± 0.004	2612 ± 6	2.557 ± 0.006	1209 ± 88	3579 ± 10	111.6 ± 0.5	111.6 ± 0.5
L4-32	1.969 ± 0.003	0.009 ± 0.005	2547 ± 8	2.520 ± 0.006	9576 ± 5084	3497 ± 12	112.4 ± 0.5	112.3 ± 0.5
L4-48	1.830 ± 0.004	0.010 ± 0.005	2624 ± 10	2.588 ± 0.006	7840 ± 3793	3611 ± 16	113.1 ± 0.7	113.0 ± 0.7
L4-79	2.403 ± 0.006	0.047 ± 0.004	2472 ± 7	2.478 ± 0.008	2101 ± 188	3404 ± 12	113.3 ± 0.7	113.2 ± 0.7
L4-93	1.657 ± 0.003	0.041 ± 0.005	2581 ± 6	2.569 ± 0.006	1724 ± 195	3561 ± 10	114.0 ± 0.5	113.9 ± 0.5
L4-102	1.368 ± 0.002	0.005 ± 0.005	2674 ± 5	2.637 ± 0.004	12533 ± 12968	3688 ± 8	113.9 ± 0.4	113.9 ± 0.4
L4-111	1.055 ± 0.002	0.097 ± 0.005	2659 ± 6	2.633 ± 0.007	471 ± 22	3673 ± 10	114.4 ± 0.6	114.3 ± 0.6
L4-114	1.002 ± 0.001	0.036 ± 0.005	2646 ± 5	2.630 ± 0.004	1206 ± 156	3659 ± 8	114.9 ± 0.4	114.8 ± 0.4
L4-117	1.248 ± 0.002	5.925 ± 0.010	1952 ± 4	2.852 ± 0.006	9.91 ± 0.02	3410 ± 13	198 ± 1	197 ± 1

^aAn asterisk (*) indicates samples were measured by the Nanjing Normal University Isotope Laboratory.

^b ^{238}U = $[^{235}\text{U}] \times 137.818 (\pm 0.65\%)$ (Hiess et al., 2012); $\delta^{234}\text{U} = ([^{234}\text{U}/^{238}\text{U}]_{\text{activity}} - 1) \times 1000$.

^c $^{230}\text{Th}/^{238}\text{U}$ activity = $1 - e^{-\lambda_{230}T} + (\delta^{234}\text{U}_{\text{measured}}/1000)[\lambda_{230}/(\lambda_{230} - \lambda_{234})](1 - e^{-(\lambda_{230} - \lambda_{234})T})$, where T is the age.

Decay constants are $9.1705 \times 10^{-6}/\text{yr}$ for ^{230}Th , $2.8221 \times 10^{-6}/\text{yr}$ for ^{234}U (Cheng et al., 2013), and $1.55125 \times 10^{-10}/\text{yr}$ for ^{238}U (Jaffey et al., 1971).

^d $\delta^{234}\text{U}_{\text{initial}}$ corrected was calculated based on ^{230}Th age (T), i.e., $\delta^{234}\text{U}_{\text{initial}} = \delta^{234}\text{U}_{\text{measured}} \times e^{\lambda_{234}T}$, where T is corrected age.

^eAge corrections, relative to before AD 1950, were calculated using an estimated atomic $^{230}\text{Th}/^{232}\text{Th}$ atomic ratio of $4 \pm 2 \times 10^{-6}$. Those are the values for material at secular equilibrium, with the crustal $^{232}\text{Th}/^{238}\text{U}$ value of 3.8. The errors are arbitrarily assumed to be 50%.

^fAnalytical errors are 2σ of the mean.

For stalagmite L4, high ^{238}U levels are $1.0\text{--}2.4 \times 10^{-6}\text{ g/g}$. For most layers (8/9), ^{232}Th content is only $0.005\text{--}0.097 \times 10^{-9}\text{ g/g}$ to yield small errors of $\pm 0.4\text{--}0.7\text{ ka}$. The exceptionally high ^{232}Th content of $5.93 \times 10^{-9}\text{ g/g}$ on subsample L4-117 causes a large error of $\pm 1.0\text{ ka}$ (Table 1). The determined ages for the top eight layers at a depth interval of 10–114 mm range from 111.6 to 114.8 ka (Fig. 3c). At a depth of 117 mm from the top, the measured age of 197 ka, dramatically different from other ages, indicates a hiatus at a depth of 115 mm. The estimated deposition rate is $36\ \mu\text{m/yr}$ for a depth interval of 0–114 mm for stalagmite L4.

LH36/L4 oxygen isotope records

We have compared the $\delta^{18}\text{O}$ results obtained from the stalagmites investigated in the present study with the previously published Lianhua–Dragon stalagmite $\delta^{18}\text{O}$ records at 60–0 ka (Dong et al., 2015, 2018a; Zhang et al., 2021a), as illustrated in Figure 4. This comparison also clearly shows an absence of significant offsets between $\delta^{18}\text{O}$ records at the overlapping growth intervals. We argue that the spliced $\delta^{18}\text{O}$ record at 115–108 ka (Fig. 5a) in the two stalagmites in this study, LH36 and L4, unambiguously reflects changes in monsoonal intensity over GI 25 and GS 25.

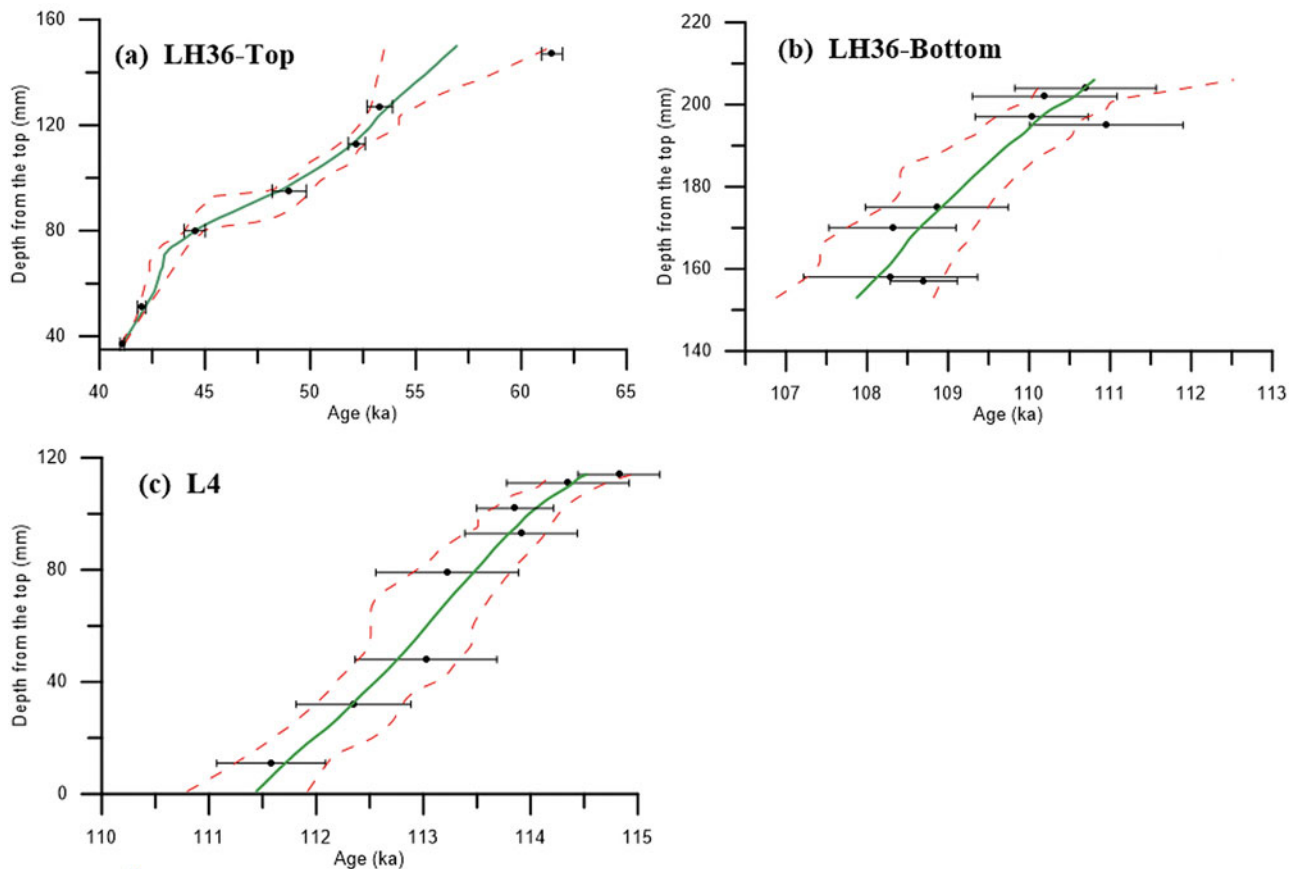


Figure 3. Plots of the age models constructed with the StalAge algorithm (Scholz and Hoffmann, 2012) for the two stalagmites, LH36 and L4. Age models for (a) the top 153 mm and (b) 153–206 mm of LH 36 and (c) L4. Black dots denote ^{230}Th dates, and horizontal bars are their 2σ errors. Green and red dashed lines are the age models with 95% confidence intervals.

The average temporal resolution of $\delta^{18}\text{O}$ data points of stalagmites LH36 and L4 plotted in Figure 5a is 27–37 yr. The stalagmite $\delta^{18}\text{O}$ record, ranging from -7.5 to -10.1 ‰, is characterized with a decreasing trend from -7.5 ‰ at 114.6 ka to -9.4 ‰ at 111.4 ka, followed by a 0.7 ka gap to 110.7 ka. The time window from 110.7 to 108.4 ka in the LH36 record is marked by two episodes of enrichment in terms of oxygen isotope ratios. The first one took place at 110.7–110.0 ka with an enrichment of 1.2‰ in $\delta^{18}\text{O}$, while the second at 109.5–108.4 ka recorded 2.5‰ enrichment. An abrupt decrease of 2.6‰ in the $\delta^{18}\text{O}$ record at 108.4 ka marked the end of the GS 25.

DISCUSSION

The interpretation of stalagmite $\delta^{18}\text{O}$ records

An essential prerequisite for using stalagmite $\delta^{18}\text{O}$ to reconstruct paleoclimate change is that stalagmites are formed under isotopic equilibrium conditions. Good between-cave reproducibility of contemporaneous $\delta^{18}\text{O}$ records at 115–108 ka for stalagmites LH36 of Lianhua Cave, L4 of Dragon Cave, and SB23 of Sanbao Cave is also expressed in Figure 5a and c. Moreover, seven stalagmite $\delta^{18}\text{O}$ records of Lianhua and Dragon Caves over the past 60 ka also show high similarities in terms of event, trend, and amplitude during overlapping growth intervals (Fig. 4b). All lines of evidence indicate a solid replication test (Dorale and Liu, 2009) and a negligible kinetic effect on

Lianhua–Dragon $\delta^{18}\text{O}$ records, which are primarily of climatic origin.

Modern instrumental observations (Zhang et al., 2004; Li et al., 2017; Wan et al., 2018), proxy records (Zhang et al., 2008; Dong et al., 2015, 2018a; Orland et al., 2015; Tan et al., 2015), and model simulations (Liu et al., 2014; Cheng et al., 2021) over the past two decades showed that Chinese stalagmite $\delta^{18}\text{O}$ variations under isotopic equilibrium conditions can generally reflect the change in monsoon intensity (Cheng et al., 2019; Zhang et al., 2021b). The regional precipitation $\delta^{18}\text{O}$ signal, eventually recorded in speleothem, in the EASM region is governed by upstream and local moisture sources (Liu et al., 2014). Rainfall amounts in southern and central China may not completely reflect monsoonal intensity (Chen et al., 2015; Liu et al., 2015). Lianhua and Dragon Caves are located in the northwest frontier of the EASM in northern China, and the regional precipitation change is very sensitive to variation in monsoon intensity, as demonstrated by instrumental data and simulated results (Liu et al., 2015). Under strong EASM conditions, high rainfall with a negative $\delta^{18}\text{O}$ value is delivered to this region (Orland et al., 2015; Tan et al., 2015). The regional Holocene stalagmite $\delta^{18}\text{O}$ records from the Lianhua (Dong et al., 2015, 2018b) and Zhenzhu Caves (Yin et al., 2017) match a pollen-based rainfall reconstruction from Bayanchagan Lake in northern China (Jiang et al., 2006; Fig. 4a) and a local dry–wet index over the past 1000 yr (CAMS, 1981), respectively. The $\delta^{18}\text{O}$ record of stalagmite L30 from Dragon Cave covaries with a quantitatively

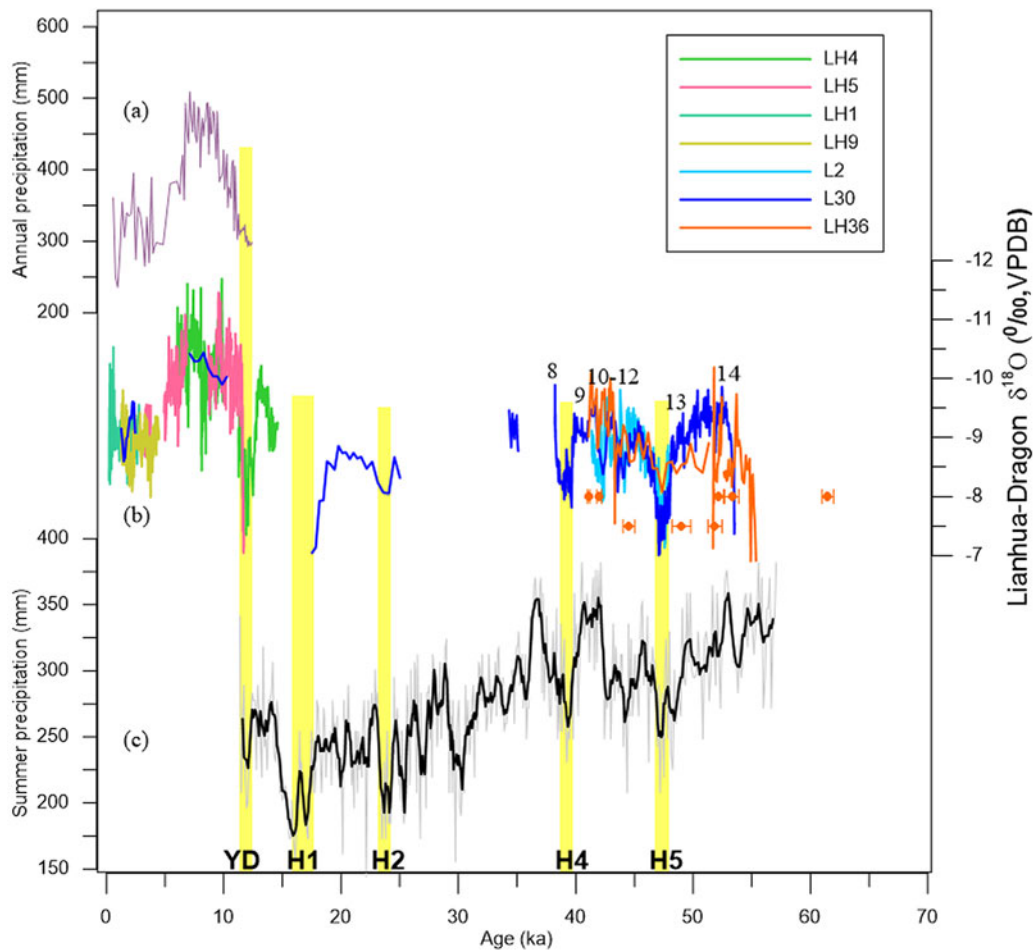


Figure 4. Comparison of the $\delta^{18}\text{O}$ for the Lianhua–Dragon stalagmites and quantitatively reconstructed monsoon rainfall records. (a) Pollen-inferred annual precipitation in Bayanchagan Lake, Inner Mongolia, northern China (Jiang et al., 2006). (b) Lianhua–Dragon $\delta^{18}\text{O}$ records (Dong et al., 2015, 2018a; Zhang et al., 2021a). Numbers denote Dansgaard–Oeschger (DO) events. (c) Quantitative reconstruction of summer rainfall in western Chinese Loess Plateau (CLP), northern China (Rao et al., 2013). Yellow bars represent weakened East Asian summer monsoon (EASM) periods at Heinrich (H) events and Younger Dryas (YD).

proxy-inferred summer rainfall record in the western CLP during the last glacial period (Dong et al., 2018a; Fig. 4). The comparison in Figure 4 and the recent proxy, empirical, and modeling studies (Liu et al., 2014; Orland et al., 2015; Cheng et al., 2019; Zhang et al., 2021b) support that the Lianhua–Dragon stalagmite $\delta^{18}\text{O}$ records can reflect monsoonal precipitation in northern China and register EASM intensity, with low value expressing a strong summer monsoon condition, and vice versa.

EASM and ISM during the GI 25 event

To better understand the regional nature of the millennial-scale climate event GI 25 during the last glacial inception, we compared the Lianhua–Dragon record with absolute dated contemporaneous stalagmites records from other Chinese caves, including Sanbao (Wang et al., 2008), Wanxiang (Johnson et al., 2006), Suozi (Zhou et al., 2008), Sanxing (Jiang et al., 2016), and Dongge (Yuan et al., 2004; Kelly et al., 2006), located in different climatic regions zones of the East Asian monsoon realm (Fig. 5). We also compared the Lianhua–Dragon $\delta^{18}\text{O}$ record with the continuous high-resolution stalagmite BT5 record from Bittoo Cave in northern India (Kathayat et al., 2016 and references

therein), where the local climate is solely influenced by the Indian summer monsoon (ISM) (Fig. 5g).

The Lianhua–Dragon $\delta^{18}\text{O}$ record in northern China shows that the millennial-scale strong monsoonal event appears to be correlated with the warm GI 25, whereas the weak monsoonal event is related to the cold GS 25 (Fig. 5a). High-resolution loess and desert sections in the CLP, near the Lianhua–Dragon region, feature the same strong monsoon, characterized by a relatively high magnetic susceptibility and organic content at GI 25 (Guan et al., 2007; Du et al., 2012). Similar results can also be expressed in other stalagmite records, including Tianmen Cave in the Tibetan Plateau, China (Cai et al., 2010) and Bittoo Cave in northern India (Kathayat et al., 2016 and references therein; Fig. 5g). The evidence generally expresses an intensified Asian summer monsoon (ASM, including the EASM and ISM) circulation at GI 25, with more monsoon precipitation permeating the interior as far as the China–Mongolia border. Subsequently, the ASM intensity abruptly decreased during the transition to GS 25 (Fig. 5a, c, and g), although this signal appears to be muted in the Dongge record (Fig. 5f).

In northwestern China, the 50-yr-resolution WX-52 $\delta^{18}\text{O}$ record with large dating uncertainty of $\pm 2\text{--}4$ ka from Wanxiang Cave documents an ^{18}O -depleted peak of $0.5\text{‰}\text{--}1.0\text{‰}$ (Johnson

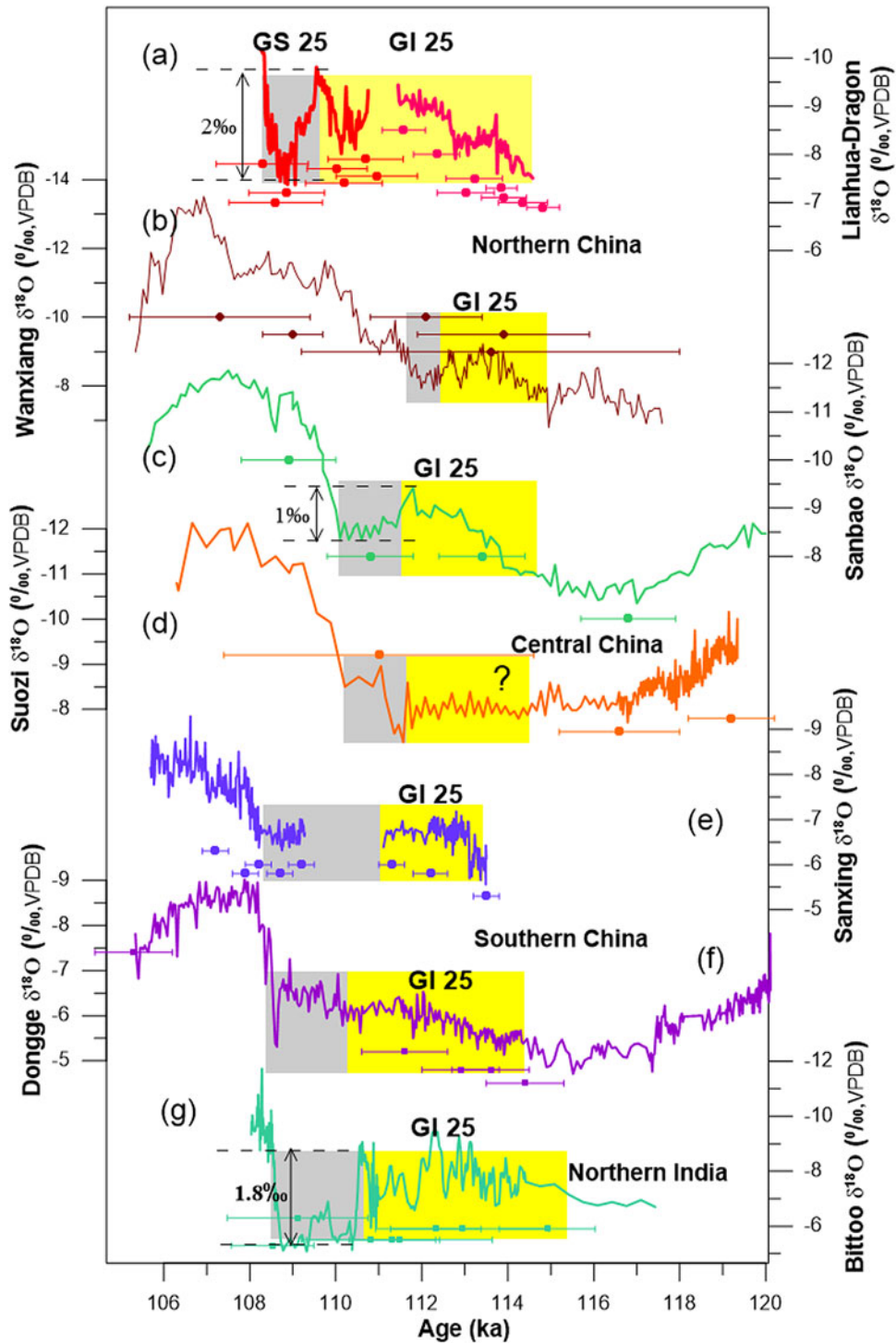


Figure 5. Stalagmite $\delta^{18}\text{O}$ records from China and northern India. Stalagmite $\delta^{18}\text{O}$ records are from (a) Lianhua–Dragon (this study) and (b) Wanxiang Caves (Johnson et al., 2006) in northern China, (c) Sanbao and (d) Suozi Caves in central China (Wang et al., 2008; Zhou et al., 2008), (e) Sanxing and (f) Dongge Caves in southwestern China (Kelly et al., 2006; Jiang et al., 2016) (Fig. 5e) show an obvious ^{18}O -depleted peak of 1.0‰ after the cold GS 26 event. A continuously 60-yr-resolved stalagmite YYZ1 $\delta^{18}\text{O}$ record

et al., 2006; Fig. 5b). Both the Sanbao $\delta^{18}\text{O}$ record from central China (Fig. 5c) and the Sanxing $\delta^{18}\text{O}$ record from southwestern China (Jiang et al., 2016) (Fig. 5e) show an obvious ^{18}O -depleted peak of 1.0‰ after the cold GS 26 event. A continuously 60-yr-resolved stalagmite YYZ1 $\delta^{18}\text{O}$ record

from Yangzi Cave in southwestern China clearly captures the monsoon event with an ^{18}O depletion of 1.0‰ (Shi et al., 2022). All stalagmite records show that this relatively small GI 25 monsoon event occurred over the Asian monsoon realm. The amplitudes of the GI 25 monsoon event recorded in

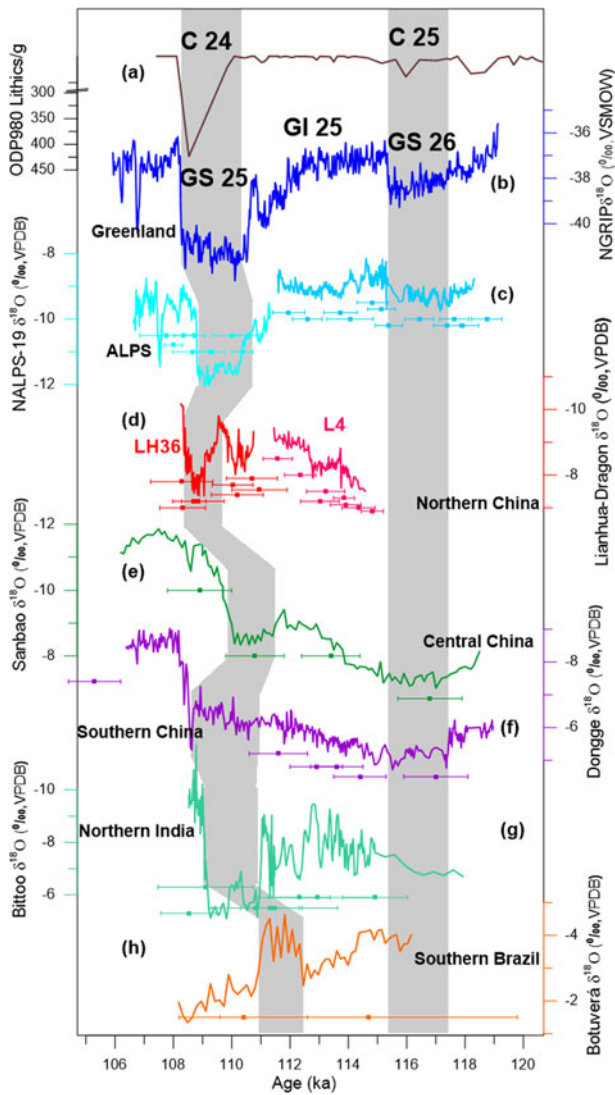


Figure 6. Comparison of stalagmites $\delta^{18}\text{O}$ time series with the Greenland ice-core and marine records during MIS 5d. (a) Lithic abundance record of Ocean Discovery Program sediment core (ODP) 980 to infer ice-rafted detritus (IRD) events (Chapman and Shackleton, 1999). (b) $\delta^{18}\text{O}$ record of NGRIP ice core based on GICC05modelext time scale (NGRIP Project Members, 2004; Wolff et al., 2010). (c) Northern Alps (NALPS) 19 stalagmite $\delta^{18}\text{O}$ records from Austria (Boch et al., 2011; Moseley et al., 2020). Chinese stalagmite $\delta^{18}\text{O}$ records from (d) Lianhua-Dragon Caves in northern China (this study), (e) Sanbao Cave in central China (Wang et al., 2008), and (f) Dongge Cave in southern China (Kelly et al., 2006). Stalagmite $\delta^{18}\text{O}$ records of (g) Bittoo Cave in northern India (Kathayat et al., 2016) and (h) Botuverá Cave in southern Brazil (Cruz et al., 2005). All records are given with their chronologies, with the exception of the marine Ocean Discovery Program sediment core (ODP) 980 record which has a shift of +2.5 ka. GI 25 represents Greenland Interstadial 25 and GS 25 and 26 are Greenland Stadials 25 and 26 (NGRIP Members, 2004), corresponding to marine events C 24 and C 25, respectively (Chapman and Shackleton, 1999; Oppo et al., 2006). Two vertical gray bars indicate two weak Asian summer monsoon (ASM) events (Wang et al., 2008), associated with GS 25 and GS 26. ^{230}Th ages with 2σ uncertainties are color coded by stalagmite.

Chinese stalagmite $\delta^{18}\text{O}$ records are 1.0‰–2.2‰ smaller than ones of subsequent rapid interstadial events (Wang et al., 2008; Jiang et al., 2016). Different from 1‰ depletion in the Sanbao record of central China (Fig. 5c), the obscure peak in the stalagmite S22 $\delta^{18}\text{O}$ record from Suozi Cave in the same district (Zhou et al., 2008; Fig. 5d) could be attributed to the different regional responses of this small strong monsoon event in the Asian

monsoon realm. Or the muted signal in Suozi Cave could be related to the complicated karst aquifer system.

The Lianhua-Dragon record (Fig. 5a) in northern China expresses an enrichment of 2‰ in ^{18}O at GS 25, 1‰ higher than that in Sanbao record (Fig. 5c) in central China and 1.5‰–2‰ higher than those of the Yangzi (Shi et al., 2022) and Dongge records (Fig. 5f) in southwestern China (Fig. 5). In northern India, the stalagmite BT5 $\delta^{18}\text{O}$ record of Bittoo Cave shows an ^{18}O enrichment of 1.8‰ at GS 25 (Fig. 5g). The different ^{18}O enrichments among stalagmite records (Fig. 5) revealed the heterogeneity of the weak regional monsoon conditions, and conditions in the fringe regions were more severe. The difference in hydroclimatic changes may partly account for the phenomenon of the muted GS 25 monsoonal events as recorded in the southern Chinese stalagmites (Kelly et al., 2006; Wu et al., 2020).

Comparison with the Greenland ice-core $\delta^{18}\text{O}$ record

High northern latitudes witnessed significant millennial-scale fluctuations in temperature during MIS 5d (114.6–108.3 ka), characterized with a warm interstadial (GI 25) and two cold stadials (GS 25 and 26) in the NGRIP ice core (NGRIP Project Members, 2004; Fig. 6b). Those events were also clearly registered in the precisely dated stalagmite $\delta^{18}\text{O}$ records from Corchia Cave, Italy (Drysdales et al., 2007) and caves in the northern Alps (NALPS) of central Europe (Boch et al., 2011; Fig. 6c). Similar millennial-scale abrupt climate events occurred along the ancient Silk Road at the beginning of the last glacial. For example, after the end of the cold GS 26 event, the Greenland air temperature rapidly increased by 5 °C in less than 100 yr at 115.3 ± 2.5 ka and maintained a warm stage until the next cold stage of GS 25 (Kindler et al., 2014). Stalagmite L4 of Dragon Cave began to deposit at 114.8 ± 0.4 ka after a hiatus, and its $\delta^{18}\text{O}$ values show a decreasing trend, suggesting an increasing EASM over the whole GI 25 event, confirmed by the Sanbao record (Wang et al., 2008; Fig. 5c). Moreover, a rapid transition into the cold GS 25 as recorded by the Lianhua-Dragon record at 109.5 ka concurred with its European counterpart in NALPS stalagmites at 110.3 ka (Boch et al., 2011; Moseley et al., 2020) and the NGRIP ice-core record at 110.6 ka within age errors (Fig. 6).

One prominent multicentennial-scale abrupt isotopic anomaly, with an amplitude of 1.2‰ that lasted for 700 yr from $110.7^{+0.6}_{-0.5}$ to $110.0^{+0.8}_{-0.4}$ ka, was first distinguished in the Lianhua-Dragon record during GI 25 (Fig. 7c). This weak-monsoon anomaly, GI 25b, separates the GI 25 event's two strong-monsoon substages, the 3.8-ka-long GI 25c and the 500-yr-long GI 25a. The multicentennial-to-millennial variations displayed in the Lianhua-Dragon record are more evident than those of the stalagmite $\delta^{18}\text{O}$ records from central and southwestern China (Fig. 5c–f). We speculate that this difference could be attributable to our study site being closer to the northern boundary of the EASM and more sensitive than other regions (Dong et al., 2015). The high-resolution $\delta^{18}\text{O}$ record from Bittoo Cave in northern India, located at the edge of the ISM, also clearly expresses the similar short-lived climate events during GI 25 (Figs. 5g and 7d).

A detailed comparison with other high-resolution sequences along the south-north longitude transect in the Northern Hemisphere over GI 25 is given in Figure 7. These intra-GI 25 strong/weak monsoon events in Figure 7c and d show a striking similarity to the corresponding two warm periods and intervening cold interval in the NGRIP ice-core $\delta^{18}\text{O}$ record (Fig. 7a). For

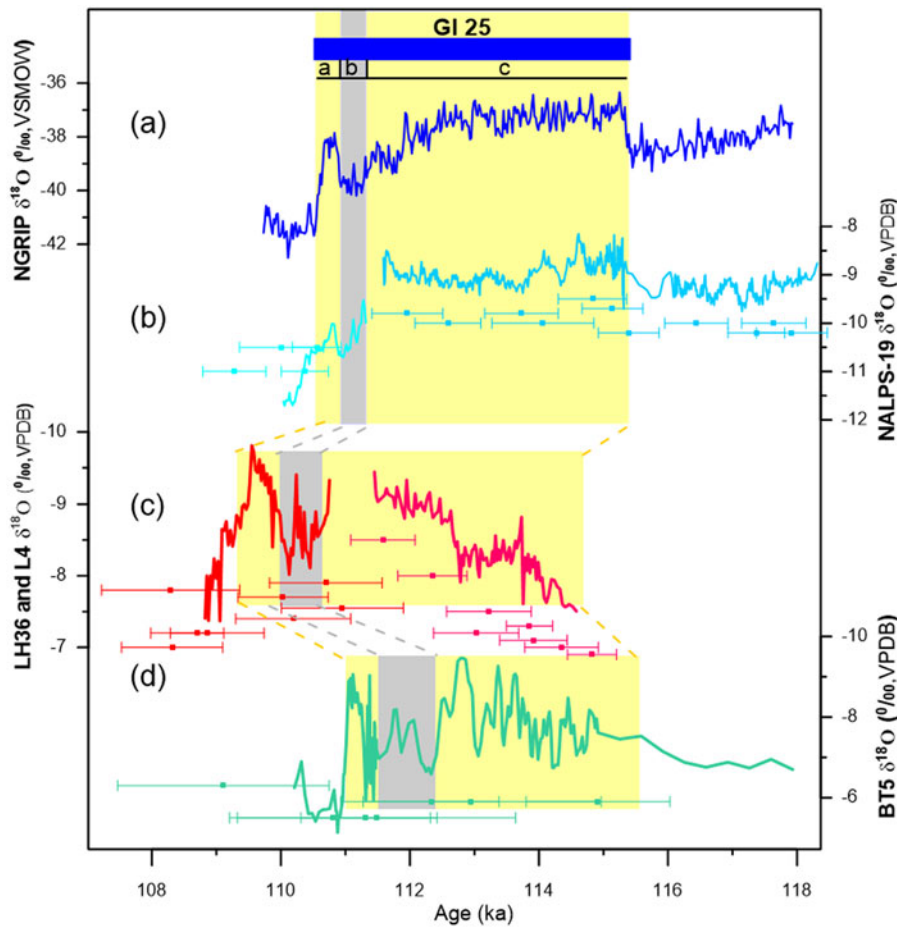


Figure 7. A detailed comparison of the centennial-scale Asian summer monsoon (ASM) variability with the high-latitude North Atlantic temperature change during the Greenland interstadial (GI) 25 event. (a) NGRIP ice $\delta^{18}\text{O}$ record with substages a, b, and c on GICC05 model time scale (NGRIP Project Members, 2004; Wolff et al., 2010). (b) Northern Alps (NALPS) 19 stalagmite $\delta^{18}\text{O}$ record from Austria (Boch et al., 2011; Moseley et al., 2020). (c) Lianhua–Dragon stalagmite $\delta^{18}\text{O}$ record from northern China. (d) Bittoo BT 5 stalagmite $\delta^{18}\text{O}$ record from northern India (Kathayat et al., 2016). Gray vertical bar denotes substage GI 25b.

example, a distinct weakening monsoon event lasting from 110.7^{+0.6} to 110.0^{+0.8} to 110.0^{-0.5} to 110.0^{-0.4} ka in the Lianhua–Dragon record (Fig. 7c) is linked to the 500 yr cold-dry excursion of GI 25b from 111.4 to 110.9 ka in the Greenland ice-core record (Fig. 7a). A short-lived aridity event occurred at 112.4–111.4 ka in northern India, revealed in the Bittoo stalagmite BT5 $\delta^{18}\text{O}$ record (Kathayat et al., 2016; Fig. 7d), matches its counterparts in NALPS stalagmite and Greenland ice-core records within dating errors (Fig. 7).

The GI 25a marks the earliest glacial “rebound-type event,” depicted as a short-lived warm reversal during the gradual cooling limb of a large GI 25 event in the NGRIP record (Capron et al., 2010, 2012; Fig. 7a). A similar feature is also documented in the European stalagmite records, expressed as a temperature increase in Figure 7b. In the Asian monsoon region, records from the Lianhua–Dragon Caves of northern China and Bittoo Cave of north India (Fig. 7c and d) show an abrupt concurrent persistent monsoonal condition during GI 25a. The 400 yr duration of this warm GI 25a in NGRIP $\delta^{18}\text{O}$ and CH_4 records (Capron et al., 2012; Rasmussen et al., 2014) matches its counterpart in the ASM region: 500 yr in the Lianhua Cave record and 400 yr in the Bittoo Cave record (Fig. 7). This concurrency indicates a strong teleconnection between the ASM and temperature change in the North Atlantic on centennial-to-millennial time scales during MIS 5d.

Interhemispheric comparison

A regional insolation-governed interhemispheric antiphasing monsoonal pattern on millennial-to-orbital scales during the

last glacial period was proposed by Wang et al. (2007), who compared stalagmite $\delta^{18}\text{O}$ records in Brazil and eastern China from 90 to 0 ka. Here we have further evaluated this relationship by using northern Chinese stalagmite $\delta^{18}\text{O}$ records. Changes in Lianhua–Dragon $\delta^{18}\text{O}$ records, concurrent with the Sanbao record, are opposite to those in the Botuverá Cave record from southern Brazil (Cruz et al., 2005) on a millennial scale. During the MIS 5d, the South American summer monsoon became very weak during the warm GI 25 and was enhanced during the cold GS 25 (Fig. 6h). Although age uncertainties of stalagmite chronologies hinder a detailed comparison, an interhemispheric antiphasing similarity is sound even for hydroclimatic changes in northern China. These observations support the bipolar seesaw hypothesis that explains the time relationship between DO and Antarctic isotope maxima events (Broecker, 1998; Barker et al., 2009).

Atlantic meridional overturning circulation (AMOC) has been proposed to explain the linkage of millennial-scale hydroclimate between the ASM and high-latitude Northern Hemisphere (Wang et al., 2001; Caballero-Gill et al., 2012; Deplazes et al., 2013; Dong et al., 2018a). The AMOC affects the oceanic transport of heat from low latitudes to the North Atlantic. In turn, it is strongly influenced by the extensive amounts of ice melt entering the North Atlantic, which attenuates the density-driven thermohaline circulation and leads to climate changes worldwide (Hemming, 2004). Such a mechanism was confirmed by a simulation that coupled the AMOC and ASM (Sun et al., 2011). Results from the International Ocean Discovery Program sediment core (ODP) 1063 suggest that AMOC was relatively unstable

on the millennial scale during the last glacial period (Böhm et al., 2015). Two prominent weak EASM anomalies in the Lianhua–Dragon and Sanbao $\delta^{18}\text{O}$ records correlate well with the North Atlantic ice-rafted detritus (IRD) events C 24 and C 25 (Chapman and Shackleton, 1999 and references therein; Fig. 6a) and their counterparts in the NGRIP record (Fig. 6b). This good alignment supports the previous hypothesis that the millennial-scale abrupt climate changes in the North Atlantic region may influence the Asian monsoonal climate through the reorganization of large-scale atmospheric circulation patterns (Porter and An, 1995; An and Porter, 1997; Wang et al., 2001). Changes in large-scale atmospheric circulations are linked to the displacement of the intertropical convergence zone, providing a potential association between the observed millennial-scale covariations in low and high latitudes (Y.J. Wang et al., 2001; Fleitmann et al., 2007; X.F. Wang et al., 2007; Zhao et al., 2010).

CONCLUSIONS

Based on 28 precise ^{230}Th dates, we provide a multidecadal-resolved stalagmite $\delta^{18}\text{O}$ record from 114.6 to 108.3 ka from two neighboring caves, Lianhua and Dragon, in Shanxi Province, northern China. The $\delta^{18}\text{O}$ records feature a strengthened monsoon interval associated with the corresponding GI 25 event and two weak monsoon events linked to cold episodes in Greenland and ice-rafting events in the North Atlantic, respectively. On the millennial time scale, our results are broadly consistent with previously published Chinese and Indian stalagmite $\delta^{18}\text{O}$ records, but directly in opposition to the stalagmite $\delta^{18}\text{O}$ record in southern Brazil. The Lianhua–Dragon record captures prominent multicentennial-to-millennial monsoon events, corresponding to the substages of intra-interstadial climate oscillations in GI 25. Our study shows the strong hydroclimate links between ASM and Northern Hemisphere high latitudes during MIS 5d.

Supplementary Material. The supplementary material for this article can be found at <https://doi.org/10.1017/qua.2022.5>

Acknowledgments. We thank two anonymous reviewers for critical and instructive comments and suggestions.

Financial Support. This work was supported by the National Natural Science Foundation of China (awards 41877287, 41472317, and 41102216). U-Th dating in the HISPEC was supported by grants from the Science Vanguard Research Program of the Ministry of Science and Technology (MOST) (109-2123-M-002-001), the Higher Education Sprout Project of the Ministry of Education (109L901001), and National Taiwan University (110L8907).

REFERENCES

- An, Z.S., Porter, S.C., 1997. Millennial-scale climatic oscillations during the last interglaciation in central China. *Geology* 25, 603–606.
- Barker, S., Diz, P., Vautravers, M.J., Pike, J., Knorr, G., Hall, I.R., Broecker, W.S., 2009. Interhemispheric Atlantic seesaw response during the last deglaciation. *Nature* 457, 1097–1102.
- Baumgartner, M., Kindler, P., Eicher, O., Floch, G., Schilt, A., Schwander, J., Spahni, R., et al., 2014. NGRIP CH_4 concentration from 120 to 10 kyr before present and its relation to a $\delta^{15}\text{N}$ temperature reconstruction from the same ice core. *Climate of the Past* 10, 903–920.
- Boch, R., Cheng, H., Spötl, C., Edwards, R.L., Wang, X., Häuselmann, P., 2011. NALPS: a precisely dated European climate record 120–60 ka. *Climate of the Past* 7, 1247–1259.
- Böhm, E., Lippold, J., Gutjahr, M., Frank, M., Blaser, P., Antz, B., Fohlmeister, J., Frank, N., Andersen, M.B., Deininger, M., 2015 Strong

and deep Atlantic meridional overturning circulation during the last glacial cycle. *Nature* 517, 73–78.

- Broecker, W.S., 1998. Paleocirculation during the last deglaciation: a bipolar seesaw? *Paleoceanography* 13, 119–121.
- Caballero-Gill, R.P., Clemens, S., Prell, W., 2012. Antarctic isotope maxima events 24 and 25 identified in benthic marine $\delta^{18}\text{O}$. *Paleoceanography* 27, PA1101.
- Cai, Y., Cheng, H., An, Z.S., Edwards, R.L., Wang, X.F., Tan, L.C., Wang, J., 2010. Large variations of oxygen isotopes in precipitation over south-central Tibet during Marine Isotope Stage 5. *Geology* 38, 243–246.
- [CAMS] Chinese Academy of Meteorological Science, 1981. *Yearly Charts of Drought/Flood in China for the Last 500-Year Period*. [In Chinese]. Sinomaps Press, Beijing.
- Capron, E., Landais, A., Chappellaz, J., Buiron, D., Fischer, H., Johnsen, S.J., Jouzel, J., Leuenberger, M., Masson-Delmotte, V., Stocker, T.F., 2012. A global picture of the first abrupt climatic event occurring during the last glacial inception. *Geophysical Research Letters* 39, L15703.
- Capron, E., Landais, A., Chappellaz, J., Schilt, A., Buiron, D., Dahl-Jensen, D., Johnsen, S.J., et al., 2010. Millennial and sub-millennial scale climatic variations recorded in polar ice cores over the last glacial period. *Climate of the Past* 6, 345–365.
- Chapman, M.R., Shackleton, N.J., 1999. Global ice-volume fluctuations, North Atlantic ice-rafting events, and deep-ocean circulation changes between 130 and 70 ka. *Geology* 27, 795–798.
- Chen, F., Xu, Q., Chen, J., Birks, H.J.B., Liu, J., Zhang, S., Jin, L., An, C., Telford, R.J., Cao, X., 2015. East Asian summer monsoon precipitation variability since the last deglaciation. *Scientific Reports* 5, 11186.
- Cheng, H., Edwards, R.L., Shen, C.-C., Polyak, V.J., Asmerom, Y., Woodhead, J., Hellstrom, J., et al., 2013. Improvements in ^{230}Th dating, ^{230}Th and ^{234}U half-life values, and U-Th isotopic measurements by multi-collector inductively coupled plasma mass spectrometry. *Earth and Planetary Science Letters* 372, 82–91.
- Cheng, H., Zhang, H., Zhao, J., Li, H., Ning, Y., Kathayat, G., 2019. Chinese stalagmite paleoclimate researches: a review and perspective. *Science China Earth Sciences* 62, 1489–1513.
- Cheng, J., Wu, H.B., Liu, Z.Y., Gu, P., Wang, J.J., Zhao, C., Li, Q., et al., 2021. Vegetation feedback causes delayed ecosystem response to East Asian summer monsoon rainfall during the Holocene. *Nature Communications* 12, 1843.
- Columbu, A., Drysdale, R., Capron, E., Woodhead, J., Waele, J.D., Sanna, L., Hellstrom, J., Bajo, P., 2017. Early last glacial intra-interstadial climate variability recorded in a Sardinian speleothem. *Quaternary Science Reviews* 169, 391–397.
- Cruz, F.W., Burns, S.J., Karmann, I., Sharp, W.D., Vuille, M., Cardoso, A.O., Ferrari, J.A., Dias, P.L.S., Viana, O., Jr., 2005. Insolation driven changes in atmospheric circulation over the past 116,000 years in subtropical Brazil. *Nature* 434, 63–66.
- Deplazes, G., Lückge, A., Peterson, L.C., Timmermann, A., Hamann, Y., Hughen, K.A., Röhl, U., et al., 2013. Links between tropical rainfall and North Atlantic climate during the last glacial period. *Nature Geoscience* 6, 213–217.
- Dong, J.G., Shen, C.-C., Kong, X.G., Wang, H.-C., Jiang, X.Y., 2015. Reconciliation of hydroclimate sequences from the Chinese Loess Plateau and low-latitude East Asian summer monsoon regions over the past 14,500 years. *Palaeogeography, Palaeoclimatology, Palaeoecology* 435, 127–135.
- Dong, J.G., Shen, C.-C., Kong, X.G., Wang, Y., Duan, F.C., 2018a. Asian monsoon dynamics at Dansgaard/Oeschger events 14–8 and Heinrich events 5–4 in northern China. *Quaternary Geochronology* 47, 72–80.
- Dong, J.G., Shen, C.-C., Kong, X.G., Wu, C.-C., Hu, H.-M., Ren, H.J., Wang, Y., 2018b. Rapid retreat of the East Asian summer monsoon in the middle Holocene and a millennial weak monsoon interval at 9 ka in northern China. *Journal of Asian Earth Sciences* 151, 31–39.
- Dorale, J., Liu, Z.H., 2009. Limitations of Hendsy test criteria in judging the paleoclimatic suitability of speleothems and the need for replication. *Journal of Cave and Karst Studies* 71, 73–80.
- Drysdale, R.N., Zanchetta, G., Hellstrom, J.C., Fallick, A.E., McDonald, J., Cartwright, I., 2007. Stalagmite evidence for the precise timing of North Atlantic cold events during the early last glacial. *Geology* 35, 77–80.

- Du, S.H., Li, B.S., Chen, M.H., Zhang, D.D., Xiang, R., Niu, D.F., Wen, X.H., Ou, X.J., 2012. Kiloyear-scale climate events and evolution during the Last Interglacial, Mu Us Desert, China. *Quaternary International* **263**, 63–70.
- EPICA Community Members, 2006. One-to-one coupling of glacial climate variability in Greenland and Antarctica. *Nature* **444**, 195–197.
- Fleitmann, D., Burns, S.J., Mangini, A., Mudelsee, M., Kramers, J., Villa, I., Neff, U., *et al.*, 2007. Holocene ITCZ and Indian monsoon dynamics recorded in stalagmites from Oman and Yemen (Socotra). *Quaternary Science Reviews* **26**, 170–188.
- Guan, Q.Y., Pan, B.T., Gao, H.S., Yuan, L.B., Wang, J.L., Huai, S., 2007. Instability characteristics of the East Asian monsoon recorded by high-resolution loess sections from the last interglacial (MIS5). *Science China Earth Sciences* **50**, 1067–1075.
- Hemming, S.R., 2004. Heinrich events: massive late Pleistocene detritus layers of the North Atlantic and their global climate imprint. *Reviews of Geophysics* **42**, RG1005.
- Hiess, J., Condon, D.J., McLean, N., Noble, S.R., 2012. $^{238}\text{U}/^{235}\text{U}$ systematics in terrestrial U-bearing minerals. *Science* **335**, 1610–1614.
- Jaffey, A.H., Flynn, K.F., Glendenin, L.E., Bentley, W.C., Essling, A.M., 1971. Precision measurement of half-lives and specific activities of U-235 and U-238. *Physical Review* **4**, 1889–1906.
- Jiang, W.Y., Guo, Z.T., Sun, X.J., Wu, H.B., Chu, G.Q., Yuan, B.Y., Hatté, C., Guiot, J., 2006. Reconstruction of climate and vegetation changes of Lake Bayanchagan (Inner Mongolia): Holocene variability of the East Asian monsoon. *Quaternary Research* **65**, 411–420.
- Jiang, X.Y., Wang, X.Y., He, Y.Q., Hu, H.-M., Li, Z.Z., Spötl, C., Shen, C.-C., 2016. Precisely dated multidecadally resolved Asian summer monsoon dynamics 113.5–86.6 thousand years ago. *Quaternary Science Reviews* **143**, 1–12.
- Johnson, K.R., Ingram, B.L., Sharp, W.D., Zhang, P.Z., 2006. East Asian summer monsoon variability during Marine Isotope Stage 5 based on speleothem $\delta^{18}\text{O}$ records from Wanxiang Cave, Central China. *Palaeogeography, Palaeoclimatology, Palaeoecology* **236**, 5–19.
- Kathayat, G., Cheng, H., Sinha, A., Spötl, C., Edwards, R.L., Zhang, H.W., Li, X.L., Yi, L., Ning, Y.F., Cai, Y.J., Liu, W.G., Breitenbach, S.F.M., 2016. Indian monsoon variability on millennial-orbital timescales. *Scientific Reports* **6**, 24374.
- Kelly, M.J., Edwards, R.L., Cheng, H., Yuan, D., Zhang, M., An, Z., 2006. High resolution characterization of the AM between 146,000 and 99,000 years B.P. from Dongge Cave, China and global correlation of events surrounding Termination II. *Palaeogeography, Palaeoclimatology, Palaeoecology* **236**, 20–38.
- Kindler, P., Guillevic, M., Baumgartner, M., Schwander, J., Landais, A., Leuenberger, M., 2014. Temperature reconstruction from 10 to 120kyr b2k from the NGRIP ice core. *Climate of the Past* **10**, 887–902.
- Landais, A., Masson-Delmotte, V., Jouzel, J., Raynaud, D., Johnsen, S., Huber, C., Leuenberger, M., Schwander, J., Minster, B., 2006. The glacial inception as recorded in the North-GRIP Greenland ice core: timing, structure and associated abrupt temperature changes. *Climate Dynamics* **26**, 273–284.
- Leuschner, D.C., Sirocko, F., 2000. The low-latitude monsoon climate during Dansgaard-Oeschger cycles and Heinrich Events. *Quaternary Science Reviews* **19**, 243–254.
- Liu, J., Chen, J., Zhang, X., Li, Y., Rao, Z., Chen, F., 2015. Holocene East Asian summer monsoon records in northern China and their inconsistency with Chinese stalagmite $\delta^{18}\text{O}$ records. *Earth-Science Reviews* **148**, 194–208.
- Liu, Z.Y., Wen, X.Y., Brady, E.C., Otto-Bliesner, B., Yu, G., Lu, H.Y., Cheng, H., *et al.*, 2014. Chinese cave records and the East Asia summer monsoon. *Quaternary Science Reviews* **83**, 115–128.
- Li, X., Cheng, H., Tan, L., Ban, F., Sinha, A., Duan, W., Li, H., *et al.*, 2017. The East Asian summer monsoon variability over the last 145 years inferred from the Shihua Cave record, North China. *Scientific Reports* **7**, 7078.
- Martin-Puertas, C., Brauer, A., Wulf, S., Lauterbach, S., Dulske, P., 2014. Annual proxy data from Lago Grande di Monticchio (southern Italy) between 76 and 112 ka: new chronological constraints and insights on abrupt climatic oscillations. *Climate of the Past* **10**, 2099–2114.
- Moseley, G.E., Spötl, C., Brandstätter, S., Erhardt, T., Luetscher, M., Edwards, R.L., 2020. NALPS19: sub-orbital-scale climate variability recorded in northern Alpine speleothems during the last glacial period. *Climate of the Past* **16**, 29–50.
- [NGRIP] North Greenland Ice Core Project Members, 2004. High-resolution re-cord of Northern Hemisphere climate extending into the last inter-glacial period. *Nature* **431**, 147–151.
- Oppo, D.W., McManus, J. F., Cullen, J.L., 2006. Evolution and demise of the Last Interglacial warmth in the subpolar North Atlantic. *Quaternary Science Reviews* **25**(23–24), 3268–3299.
- Orland, I.J., Edwards, R.L., Cheng, H., Kozdon, R., Cross, M., Valley, J.W., 2015. Direct measurements of deglacial monsoon strength in a Chinese stalagmite. *Geology* **43**, 555–558.
- Porter, S.C., An, Z.S., 1995. Correlation between climate events in the North Atlantic and China during the last glaciation. *Nature* **375**, 305–308.
- Rao, Z.G., Chen, F.H., Cheng, H., Liu, W.G., Wang, G., Lai, Z.P., Bloemendal, J., 2013. High-resolution summer precipitation variations in the western Chinese Loess Plateau during the last glacial. *Scientific Reports* **3**, 2785.
- Rasmussen, S.O., Bigler, M., Blockley, S.P., Blunier, T., Buchardt, S.L., Clausen, H.B., Cvijanovic, I., *et al.*, 2014. A stratigraphic framework for abrupt climatic changes during the Last Glacial period based on three synchronized Greenland ice-core records: refining and extending the INTIMATE event stratigraphy. *Quaternary Science Reviews* **106**, 14–28.
- Scholz, D., Hoffmann, D.L., Hellstrom, J., Bamsey, C.B., 2012. A comparison of different methods for speleothem age modelling. *Quaternary Geochronology* **14**, 94–104.
- Shao, Q., Li, C., Huang, M., Liao, Z., Arps, J., Huang, C., Chou, Y., Kong, X.G., 2019. Interactive programs of MC-ICPMS data processing for $^{230}\text{Th}/\text{U}$ geochronology. *Quaternary Geochronology* **51**, 43–52.
- Shen, C.-C., Cheng, H., Edwards, R.L., Moran, S.B., Edmonds, H.N., Hoff, J.A., Thomas, R.B., 2003. Measurement of attogram quantities of ^{231}Pa in dissolved and particulate fractions of seawater by isotope dilution thermal ionization mass spectroscopy. *Analytical Chemistry* **75**, 1075–1079.
- Shen, C.-C., Lawrence Edwards, R., Cheng, H., Dorale, J.A., Thomas, R.B., Bradley Moran, S., Weinstein, S.E., Edmonds, H.N., 2002. Uranium and thorium isotopic and concentration measurements by magnetic sector inductively coupled plasma mass spectrometry. *Chemical Geology* **185**, 165–178.
- Shen, C.-C., Wu, C.-C., Cheng, H., Edwards, R.L., Hsieh, Y.-T., Gallet, S., Chang, C.-C., *et al.*, 2012. High-precision and high-resolution carbonate ^{230}Th dating by MC-ICP-MS with SEM protocols. *Geochimica et Cosmochimica Acta* **99**, 71–86.
- Shi, X., Yang, Y., Cheng, H., Zhao, J.Y., Li, T.Y., Lei, L., Liang, S., Feng, X.X., Edwards, R.L., 2022. Influences on Asian summer monsoon during Dansgaard-Oeschger events 19 to 25 (70–115kyr B.P.). *Palaeogeography, Palaeoclimatology, Palaeoecology* **587**, 110798.
- Sun, Y., Clemens, S.C., Morrill, C., Lin, X., Wang, X., An, Z., 2011. Influence of Atlantic meridional overturning circulation on the East Asian winter monsoon. *Nature Geoscience* **5**, 46–49.
- Tan, L., Cai, Y., Cheng, H., Lawrence Edwards, R., Shen, C.-C., Gao, Y., An, Z., 2015. Climate significance of speleothem $\delta^{18}\text{O}$ from central China on decadal timescale. *Journal of Asian Earth Sciences* **106**, 150–155.
- Voelker, A.H.L., 2002. Global distribution of centennial-scale records for Marine Isotope Stage (MIS) 3: a database. *Quaternary Science Reviews* **21**, 1185–1212.
- Wang, X.F., Auler, A.S., Edwards, R.L., Cheng, H., Ito, E., Wang, Y.J., Kong, X.G., Solheid, M., 2007. Millennial-scale precipitation changes in southern Brazil over the past 90,000 years. *Geophysical Research Letters* **34**. <http://dx.doi.org/10.1029/2007GL031149>.
- Wang, Y.J., Cheng, H., Edwards, R.L., An, Z.S., Wu, J.Y., Shen, C.-C., Dorale, J.A., 2001. A high-resolution absolute-dated late Pleistocene monsoon record from Hulu Cave, China. *Science* **294**, 2345–2348.
- Wang, Y.J., Cheng, H., Edwards, R.L., Kong, X.G., Shao, X.H., Chen, S.T., Wu, J.Y., Jiang, X.Y., Wang, X.F., An, Z.S., 2008. Millennial- and orbital-scale changes in the East Asian monsoon over the past 224,000 years. *Nature* **451**, 1090–1093.
- Wan, H., Liu, W., Xing, M., 2018. Isotopic composition of atmospheric precipitation and its tracing significance in the Laohequ Basin, Loess plateau, China. *Science of the Total Environment* **640–641**, 989–996.

- Wolff, E.W., Chappellaz, J., Blunier, T., Rasmussen, S.O., Svensson, A., 2010. Millennial-scale variability during the last glacial: the ice core record. *Quaternary Science Reviews* **29**, 2828–2838.
- Wu, Y., Li, T.Y., Yu, T.-L., Shen, C.-C., Chen, C.-J., Zhang, J., Li, J.Y., Wang, T., Huang, R., Xiao, S.Y., 2020. Variation of the Asian summer monsoon since the last glacial-interglacial recorded in a stalagmite from southwest China. *Quaternary Science Reviews* **234**, 106261.
- Yin, J.J., Li, H. C., Rao, Z.G., Shen, C.C., Mii, H.S., Pillutla, R.K., Hu, M., Li, Y.X., Feng, X.H., 2017. Variations of monsoonal rain and vegetation during the past millennium in Tianguai Mountain, north China reflected by stalagmite $\delta^{18}\text{O}$ and $\delta^{13}\text{C}$ records from Zhenzhu Cave. *Quaternary International* **447**, 89–101.
- Yuan, D.X., Cheng, H., Edwards, R.L., Dykoski, C.A., Kelly, M.J., Zhang, M.L., Qin, J.M., *et al.*, 2004. Timing, duration, and transitions of the last interglacial Asian monsoon. *Science* **304**, 575–578.
- Zhang, H., Huang, W., Jiang, Y., Chen, Z.Y., Shen, C.-C., Dong, J.G., 2021a. Structure characteristics of DO12 climate abrupt event: evidence from the stalagmite record in northern China. *Acta Sedimentologica Sinica*. <https://doi.org/10.14027/j.issn.1000-0550.2021.005>.
- Zhang, H.W., Zhang, X., Cai, Y.J., Sinha, A., Spätl, C., Baker, J., Kathayat, G., *et al.*, 2021b. A data-model comparison pinpoints Holocene spatiotemporal pattern of East Asian summer monsoon. *Quaternary Science Reviews* **261**, 106911.
- Zhang, P.Z., Cheng, H., Edwards, R.L., Chen, F.H., Wang, Y.J., Yang, X.L., Liu, J., *et al.*, 2008. A test of climate, sun, and culture relationships from an 1810-year Chinese cave record. *Science* **322**, 940–942.
- Zhang, P.Z., Chen, Y.M., Johnson, K.R., Chen, F.H., Ingram, B.L., Zhang, X.L., Zhang, C.J., Wang, S.M., Pang, F.S., Long, L.D., 2004. Environmental significance Wudu Wanxiang Cave dripping with modern stalagmite isotope. *Chinese Science Bulletin* **49**, 1529–1531.
- Zhang, X., Xiao, H.Y., Chou, Y.-C., Cai, B.G., Lone, M.A., Shen, C.-C., Jiang, X.Y., 2020. A detailed East Asian monsoon history of Greenland Interstadial 21 in southeastern China. *Palaeogeography, Palaeoclimatology, Palaeoecology* **552**, 109752.
- Zhao, K., Wang, Y.J., Edwards, R.L., Cheng, H., Liu, D.B., 2010. High-resolution stalagmite $\delta^{18}\text{O}$ records of Asian monsoon changes in central and southern China spanning the MIS 3/2 transition. *Earth and Planetary Sciences Letters* **298**, 191–198.
- Zhou, H., Zhao, J.-X., Zhang, P.Z., Shen, C.-C., Chi, B.Q., Feng, Y.X., Lin, Y., Guan, H.Z., You, C.-F., 2008. Decoupling of stalagmite-derived Asian summer monsoon records from North Atlantic temperature change during marine oxygen isotope stage 5d. *Quaternary Research* **70**, 315–321.